Institute of Space and Aeronautical Science, University of Tokyo
Report No. 544, September 1976

A Study of Transient Thermal Response of Ablation Materials

By

Norio ARAI

Summary: A thermal analysis for transient response of ablating materials made of high molecular compounds is developed on the basis of the two-layer thermal model by use of an appropriate numerical method, where the assumptions of quasi-steady boundary layer flow and the equilibrium vaporization at the ablating surface are employed.

Numerical computation is carried for an ablating blunt body of revolution made of Teflon with an emphasis laid on the effect of the second-order transition—i.e., the gel layer. It is shown that the transient internal temperature near the ablating surface is diminished considerably by the existence of the gel layer.

Comparison of the numerical results with the experimental data reveals a remarkable fact that the single-layer thermal model does not predict the real feature of the transient thermal field, while the two-layer thermal model agrees well with the experiment, thus confirming the validity of the present approach.

NOMENCLATURE

A_i, B_i, C_i, D_i coefficients in Eq. (5.2.1)
a, b, c constants in Eq. (4.2)
B mass-addition parameter defined by Eq. (3.15)
C_p specific heat
D binary diffusion coefficient
H total enthalpy
h_v energy required to ablate unit mass of body
h_m energy required to phase transion
k thermal conductivity
L thickness of the solid layer in x-direction or number of divisions in χ-direction or ξ-direction
L_0 initial body length
M number of division in r-direction
$\dot{m}$ ablation rate
p pressure
q_i heat flux across inside surface (Fig. 2)
q_0 heat flux across outside surface (Fig. 2)
R_b radius of curvature of base curve
R_e Reynolds number

r radial position (Fig. 1)
St Stanton number defined by Eq. (3.16)
s recession depth in axial direction
$\dot{s}$ $=\partial s/\partial t$
T temperature
T_m phase transition temperature
t time
t_g transition time
v velocity normal to the surface
x axial position (Fig. 1)
x_i axial position of the original surface (Fig. 1)
α thermal diffusivity
δ boundary layer thickness
δ_i angle between local interface tangent in meridian plane and axis of symmetry
δ_s angle between local surface tangent in meridian plane and axis of symmetry (Fig. 2)
δ_T thermal thickness
$\delta_{t=100}$ thermal thickness at $t=100$ sec. defined by Eq. (6.1)
ζ distance measured along a meridian line from the stagnation point (Fig. 2)
θ thickness of the gel layer in axial direction (Fig. 1)
$\dot{\theta}$ $=\partial\theta/\partial t$
ξ transformed geometric variable defined by Eq. (2.5)
ρ material density of the ablating body
χ transformed geometric variable defined by Eq. (2.2)
Ψ ratio of the heating rate with mass addition to the heating rate without mass addition
μ viscosity
ν kinematic viscosity $(=\mu/\rho)$

Subscripts:

$B=0$ conditions for no mass addition
i initial conditions
m conditions of phase transition
n components normal to local surface
s conditions at inside surface of a control surface
st stagnation conditions in free stream
t components tangential to local surface in meridian plane
w conditions at outside surface of a control surface
1 conditions in gel layer
2 conditions in solid layer
∞ conditions in free stream
g conditions at outside surface of a body

1. Introduction

At high speed re-entry of space vehicles to atmospheric environments ablation is one of the practical methods to alleviate severe aerodynamic heating. The device of heat shield by use of the ablation is, of course, to sublimate or to melt surface material of the vehicles, so that a large amount of heat from boundary layer is absorbed efficiently in the latent heat (e.g., liquefaction, vaporization etc.) for phase change of the material so as to diminish the heat conducting inside the vehicles considerably.

A number of studies [*1*], [*2*], [*3*], [*4*] have been developed with the assumption of steady ablation and comprehensive results were presented. However, since the ablation is a very complicated phenomenon associated with coupling of the non-equilibrium chemical process with the aerodynamic one involving the change in body shape with time, it seems more realistic to consider that it is in general an unsteady phenomenon, although it may attain to the steady state only in the case of a semi-infinite length body being exposed in a uniform high-enthalpy stream for a long time.

In the design of an ablative heat-shield system, estimation of the ablation rate must be of a primary interest to evaluate total mass loss and change in body shape with time. However, considering that the ultimate purpose of the ablative heat shield is to keep the internal temperature of the space vehicles at a safety level during the time of re-entry, the transient heat conduction characteristic of the ablator itself may be one of the significant factors in selection of quality and determination of thickness of the materials as well as its chemicophysical properties such as the ablation rate and the latent heat, etc. In this sense, it seems to be of another point of interest to investigate the transient thermal response of the ablative materials.

There are a few simple analyses [*5*], [*6*] for one-dimensional quasi-steady ablation. These approaches, though unrealistic in practical applications, seem to offer some useful aspects on transient thermal response of the ablators.

In the analytical approaches [*7*], [*8*], [*9*], [*10*] developed under the assumption of quasi-steady ablation for axisymmetric blunt-nosed bodies, the change in body shape with time is taken into account while the diffusion of heat in the direction tangential to the surface is neglected inside the ablator. Because of this, the range of applicability of these approaches seems to be restricted to the vicinity of the stagnation point.

On the other hand, numerical analyses were presented by Friedman et al. [*11*] for an ablating thrust chamber wall of a rocket engine and by Popper et al. [*12*] and by Tompkins et al. [*13*], respectively, for ablating axisymmetric blunt-nosed bodies, where the effect of change in surface geometry on transient thermal response is taken into account reasonably. Several examples calculated to demonstrate the validity of the analyses are shown to be in good agreement with experimental results in each case.

As to the ablators made of high-molecular compounds such as Teflon (Polytetra-

fluoroethylene) for instance, it is well known that there exists a second order transition temperature at which the solid material changes its physical properties very rapidly. This transition may be considered as melting and, in the case of Teflon, the significant change occurs in the thermal conductivity while the other properties remain almost unchanged. The melted Teflon is called gel layer in the present paper, since its viscosity is so large that the fluidity can be essentially neglected, though it might be a liquid.

Most of the existing theories made on ablation of Teflon are developed by use of the single-layer thermal model, where existence of the gel layer is ignord. However, it must be noted that the single-layer model will modify the real feature of the thermal field in the ablators, resulting in a considerable error in ablation characteristics because of the significant difference of thermal conductivity between gel layer and solid Teflon.

Despite of this circumstance, there seems to exist few previous theoretical study on transient thermal response by use of the two-layer thermal model except for a simple analysis proposed by Nomura [*14*] and even the empirical information is eager. This simple approach is essentially one-dimensional in which the initial temperature distribution is assumed to be given a priori. However, the result is shown to be in agreement with the experiment.

It is the purpose of the present paper to propose a numerical approach to transient thermal response of the ablating materials made of high molecular compounds. With a particular emphasis laid on the effects of the second order transition and the transverse diffusion of heat on the overall behavior of the transient temperature distribution inside the ablating material, the formulation is made by use of the two-layer thermal model under the assumption that the boundary layer flow is quasi-steady and the vaporization at the ablating surface is in equilibrium. Numerical calculations are carried out for a Teflon model by use of A. D. I. method.

Measurement of instantaneous internal temperature distributions in the hemisphere-cylinder model made of Teflon is carried out and the results are compared with the theoretical ones in order to confirm effectiveness of the gel layer.

2. Fundamental Equation

2.1. Basic Assumptions

Teflon is milk-white, waxy and partially crystaline (up to 80%) at the temperature below 327°C. A major phase transition usually called the "melting" point occurs at this temperature and the melted Teflon is amorphous and transparent. Although the melted Teflon should be considered as a liquid, its viscosity remains to be very high order of magnitude (for example, 10^{11} poise in the temperature range from 330 to 390°C), so that the fluidity of the molten may be neglected. In this sense, the molten layer is called as gel layer.

As pointed out by Nomura [*14*], the difference of thermal diffusivity α between the solid Teflon and the gel layer is little dependent on specific heat C_p and density ρ, but is mainly dependent on thermal conductivity k. When the second order

transition temperature T_m ($=327°C$) is approached, physical properties of Teflon change rapidly.

Based on the physical characteristcs of Teflon in solid and gel phases, the basic assumptions made in the present development may be summarized as follows;

(1) ablating material consists of two layers, namely, the gel layer and the solid (two layer thermal model).
(2) thermal properties are constant in each layer.
(3) fluidity of the gel layer is neglected because of its large viscosity (10^{11} poise).
(4) boundary layer flow on the ablating surface may be treated as quasi-steady (see Appendix).

2.2. *Heat Conduction Equation*

In the cylindrical coordinates system (Fig. 1), the unsteady heat conduction equation for an axisymmetric body with constant thermal diffusivity is given as

$$\frac{\partial T}{\partial t}=\alpha\left(\frac{\partial^2 T}{\partial r^2}+\frac{1}{r}\frac{\partial T}{\partial r}+\frac{\partial^2 T}{\partial x^2}\right), \tag{2.1}$$

where T, t and α denotes temperature, time and thermal diffusivity, respectively.

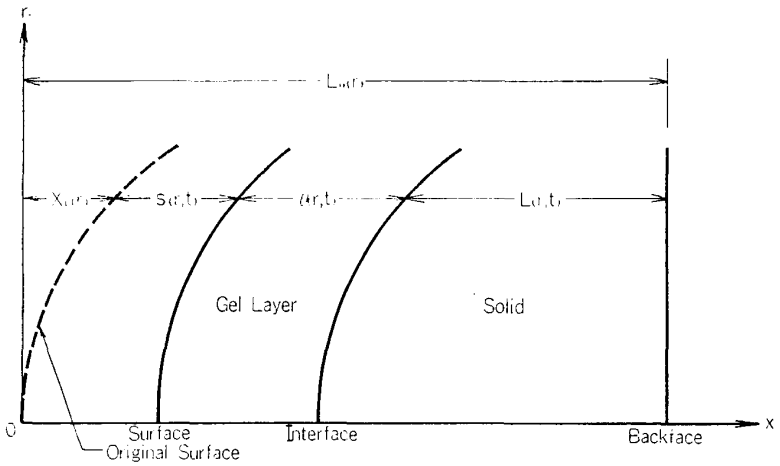

FIG. 1. Schematic Diagram of the Coordinate System.

2.3. *Transformation of Fundamental Equation*

For heat conduction problems involving surface recession, it is convenient to use a coordinate system that is fixed at the moving surface. For axisymmetric case it can be done by slight modification of the method proposed by Landau [*15*] for the one-dimensional case.

Fig. 1 shows a schematic diagram in the transformed coordinate system for an axisymmetric body. The spatial coordinates (r, x) are transformed into (r, χ) by the following expression,

$$\chi=\frac{x-(x_i+s)}{\theta}-1, \tag{2.2}$$

where x_i is the axial position of the original surface at a given radius, s is the

change in the axial position from its initial position due to surface recession and θ is the thickness of the gel layer measured in the direction of x-axis.

Thus, the instantaneous receding surface of the ablating body is denoted by $\chi=-1$, the interface between the gel layer and the solid by $\chi=0$, and the back surface is given by $\chi=L/\theta$. That is

$$\begin{aligned} -1\leq\chi\leq 0 \qquad & \text{for gel layer,} \\ 0\leq\chi\leq\frac{L}{\theta} \qquad & \text{for solid layer,} \end{aligned}$$

where L is the thickness of the solid layer in the direction of x-axis.

The chain rule of differentiation appropriate to the transformation of the variable may be summarized as

$$\left.\begin{aligned} \left(\frac{\partial}{\partial t}\right)_{r,x} &= \left(\frac{\partial}{\partial t}\right)_{r,\chi} - \frac{1}{\theta}\left\{\frac{\partial s}{\partial t}+(\chi+1)\frac{\partial\theta}{\partial t}\right\}\left(\frac{\partial}{\partial\chi}\right)_{r,t}, \\ \left(\frac{\partial}{\partial x}\right)_{r,t} &= \frac{1}{\theta}\left(\frac{\partial}{\partial\chi}\right)_{r,t}, \\ \left(\frac{\partial^2}{\partial x^2}\right)_{r,t} &= \frac{1}{\theta^2}\left(\frac{\partial^2}{\partial\chi^2}\right)_{r,t}, \\ \left(\frac{\partial}{\partial r}\right)_{x,t} &= \left(\frac{\partial}{\partial r}\right)_{\chi,t} - \frac{A}{\theta}\left(\frac{\partial}{\partial\chi}\right)_{r,t}, \\ \left(\frac{\partial^2}{\partial r^2}\right)_{x,t} &= \left(\frac{\partial^2}{\partial r^2}\right)_{\chi,t} - \frac{2A}{\theta}\left(\frac{\partial^2}{\partial\chi\partial r}\right)_{t} + \frac{A^2}{\theta^2}\left(\frac{\partial^2}{\partial\chi^2}\right)_{r,t} \\ &\quad + \frac{1}{\theta}\left(\frac{2A}{\theta}\frac{\partial\theta}{\partial r}-\frac{\partial A}{\partial r}\right)\left(\frac{\partial}{\partial\chi}\right)_{r,t}, \\ A &= \frac{dx_i}{dr}+\frac{\partial s}{\partial r}+(\chi+1)\frac{\partial\theta}{\partial r}. \end{aligned}\right\} \tag{2.3}$$

By use of Eq. (2.3), the fundamental equation, Eq. (2.1), can be reduced to

$$\begin{aligned} \frac{\partial T}{\partial t} &= \alpha\left(\frac{\partial^2 T}{\partial r^2}+\frac{1}{r}\frac{\partial T}{\partial r}\right) \\ &\quad + \frac{1}{\theta}\frac{\partial T}{\partial\chi}\left\{\frac{\partial s}{\partial t}+(\chi+1)\frac{\partial\theta}{\partial t}-\frac{\alpha}{r}A-\alpha\left(\frac{\partial A}{\partial r}-\frac{2A}{\theta}\frac{\partial\theta}{\partial r}\right)\right\} \\ &\quad + \frac{\alpha}{\theta^2}\frac{\partial^2 T}{\partial\chi^2}(1+A^2)-\frac{2\alpha A}{\theta}\frac{\partial^2 T}{\partial\chi\partial r}. \end{aligned} \tag{2.4}$$

The spatial coordinates (r, x) for the solid layer can be further simplified into (r, ξ) by introducing the transformation

$$\xi=\frac{\chi}{L/\theta}, \tag{2.5}$$

where $\xi=0$ indicates the interface between the gel layer and the solid layer and the backface is denoted by $\xi=1$, that is

$$0 \leq \xi \leq 1 \qquad \text{for solid layer.}$$

The chain rule of differentiation appropriate to this transformation may be summarized as

$$\left.\begin{aligned}
&\left(\frac{\partial}{\partial t}\right)_{r,\chi}=\left(\frac{\partial}{\partial t}\right)_{r,\xi}+\xi\left(\frac{1}{\theta}\frac{\partial\theta}{\partial t}-\frac{1}{L}\frac{\partial L}{\partial t}\right)\left(\frac{\partial}{\partial\xi}\right)_{r,t},\\
&\left(\frac{\partial}{\partial\chi}\right)_{r,t}=\frac{\theta}{L}\left(\frac{\partial}{\partial\xi}\right)_{r,t},\\
&\left(\frac{\partial^2}{\partial\chi^2}\right)_{r,t}=\frac{\theta^2}{L^2}\left(\frac{\partial^2}{\partial\xi^2}\right)_{r,t},\\
&\left(\frac{\partial^2}{\partial\chi\partial r}\right)_{t}=\frac{\theta}{L}\left(\frac{1}{\theta}\frac{\partial\theta}{\partial r}-\frac{1}{L}\frac{\partial L}{\partial r}\right)\left(\frac{\partial}{\partial\xi}\right)_{r,t}+\frac{\theta}{L}\left(\frac{\partial^2}{\partial\xi\partial r}\right)_{t}\\
&\qquad+\frac{\theta\xi}{L}\left(\frac{1}{\theta}\frac{\partial\theta}{\partial r}-\frac{1}{L}\frac{\partial L}{\partial r}\right)\left(\frac{\partial^2}{\partial\xi^2}\right)_{r,t},\\
&\left(\frac{\partial}{\partial r}\right)_{\chi,t}=\left(\frac{\partial}{\partial r}\right)_{\xi,t}+\xi\left(\frac{1}{\theta}\frac{\partial\theta}{\partial r}-\frac{1}{L}\frac{\partial L}{\partial r}\right)\left(\frac{\partial}{\partial\xi}\right)_{r,t},\\
&\left(\frac{\partial^2}{\partial r^2}\right)_{\chi,t}=\left(\frac{\partial^2}{\partial r^2}\right)_{\xi,t}+2\xi\left(\frac{1}{\theta}\frac{\partial\theta}{\partial r}-\frac{1}{L}\frac{\partial L}{\partial r}\right)\left(\frac{\partial^2}{\partial\xi\partial r}\right)_{t}\\
&\qquad+\xi\left\{\frac{1}{\theta}\frac{\partial^2\theta}{\partial r^2}-\frac{2}{\theta L}\frac{\partial\theta}{\partial r}\frac{\partial L}{\partial r}+\frac{2}{L^2}\left(\frac{\partial L}{\partial r}\right)^2-\frac{1}{L}\frac{\partial^2 L}{\partial r^2}\right\}\left(\frac{\partial}{\partial\xi}\right)_{r,t}\\
&\qquad+\xi^2\left(\frac{1}{\theta}\frac{\partial\theta}{\partial r}-\frac{1}{L}\frac{\partial L}{\partial r}\right)^2\left(\frac{\partial^2}{\partial\xi^2}\right)_{r,t}.
\end{aligned}\right\} \tag{2.6}$$

Thus, the basic equation associated with the solid layer can be further reduced to

$$\begin{aligned}
\frac{\partial T}{\partial t}=&\alpha\left(\frac{\partial^2 T}{\partial r^2}+\frac{1}{r}\frac{\partial T}{\partial r}\right)\\
&+\frac{\partial T}{\partial\xi}\left\{\alpha\xi\left(\frac{1}{\theta}\frac{\partial^2\theta}{\partial r^2}-\frac{1}{L}\frac{\partial^2 T}{\partial r^2}\right)+\frac{1-\xi}{L}\left(\frac{\partial s}{\partial t}+\frac{\partial\theta}{\partial t}\right)\right.\\
&\qquad+\frac{\alpha}{\theta}\left(\frac{L\xi}{r}-2A'-2\xi\frac{\partial L}{\partial r}-\frac{L\xi}{\theta}\frac{\partial\theta}{\partial r}\right)\frac{\partial}{\partial r}\left(\frac{\theta}{L}\right)\\
&\qquad\left.+\alpha\cdot\frac{1}{L}\left(\frac{2A'}{\theta}\frac{\partial\theta}{\partial r}-\frac{A'}{r}-\frac{\partial A'}{\partial r}\right)\right\}\\
&+\alpha\frac{\partial^2 T}{\partial\xi^2}\left\{\frac{1}{L^2}+\left[\frac{L\xi}{\theta}\frac{\partial}{\partial r}\left(\frac{\theta}{L}\right)-\frac{A'}{L}\right]^2\right\}\\
&+2\alpha\frac{\partial^2 T}{\partial\xi\partial r}\left\{\frac{L\xi}{\theta}\frac{\partial}{\partial r}\left(\frac{\theta}{L}\right)-\frac{A'}{L}\right\},
\end{aligned} \tag{2.7}$$

where

$$\begin{aligned}
A'&=\frac{dx_i}{dr}+\frac{\partial s}{\partial r}+\left(\frac{L}{\theta}\xi+1\right)\frac{\partial\theta}{\partial r},\\
L&=L_0-(x_i+s+\theta).
\end{aligned}$$

Therefore, the governing equation is given by Eq. (2.4) for the gel layer and by Eq. (2.7) for the solid layer.

3. Initial Conditions and Boundary Conditions

3.1. Initial Conditions

The initial conditions that must be specified are the temperature distribution, mass-transfer rate, and the body shape. For the most cases of interest, it may be reasonable to assume that the initial temperature distribution is uniform and the initial mass-transfer rate is zero. Those are

$$T(r, \chi, 0)=T_i, \tag{3.1}$$

$$\dot{m}_i=0, \tag{3.2}$$

3.2. Boundary Conditions

3.2.1. Boundary Conditions on the Ablating Surface

Fig. 2 shows a control surface with unit area set up on the instantaneous ablating surface ($\chi=-1$), where q_0 denotes the heat flux vector transfering from the boundary layer flow and q_i is the heat flux vector conducting into the gel layer. Due to the transverse thermal conduction within the body q_i is in general not in the same direction as q_0.

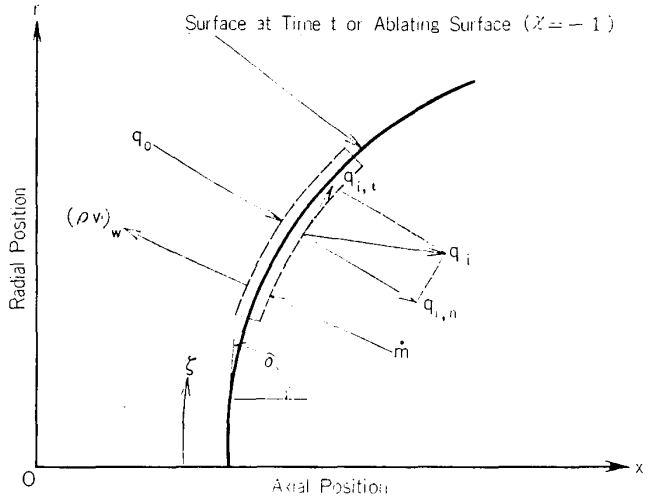

FIG. 2. Description of Boundary Conditions.

Heat transfer balance across the control surface may be given as

$$q_{i,n}=q_{0,n}-\dot{m}h_v, \tag{3.3a}$$

$$\dot{m}=\rho_1\frac{\partial s}{\partial t}\sin\delta_s, \tag{3.3b}$$

where $q_{i,n}$ and $q_{0,n}$ are the components of q_i and q_0, normal to the local surface,

respectively, and ρ_1 is the material density of the ablating body. h_v is the energy required for phase change of unit mass of the body and δ_s is the angle local surface in a meridian plane makes with the x-axis. Moreover, the following expression can be obtained from the geometrical relation of an ablating body (See Fig. 1 and Fig. 2).

$$\begin{aligned}\cot\delta_s &= -\frac{\partial}{\partial r}(L+\theta)\\ &= -\frac{\partial}{\partial r}(L_0-x_i-s)\\ &= A-\frac{dL_0}{dr},\end{aligned} \tag{3.4}$$

where L_0 is the initial body length.

The components of the heat flux vector just inside of the control surface can be expressed, respectively, as

$$-\left(k_1\frac{\partial T_1}{\partial x}\right)_s = q_{i,t}\cos\delta_s + q_{i,n}\sin\delta_s, \tag{3.5a}$$

$$-\left(k_1\frac{\partial T_1}{\partial r}\right)_s = q_{i,t}\sin\delta_s - q_{i,n}\cos\delta_s, \tag{3.5b}$$

where k_1 is the thermal conductivity in the gel layer and the subscript s means the conditions just inside of the control surface. Elimination of $q_{i,t}$ from Eq. (3.5) leads to

$$-\left(k_1\frac{\partial T_1}{\partial x}\right)_s \sin\delta_s + \left(k_1\frac{\partial T_1}{\partial r}\right)_s \cos\delta_s = q_{i,n}. \tag{3.6}$$

Therefore, Eq. (3.6) can be reexpressed by use of Eqs. (2.3) and (3.3) as

$$\begin{aligned}&-\frac{1}{\theta}\left(k_1\frac{\partial T_1}{\partial \chi}\right)_{\chi=-1}\left(1+\frac{dL_0}{dr}\sin\delta_s\cdot\cos\delta_s\right)\\ &\quad+\left(k_1\frac{\partial T_1}{\partial r}\right)_{\chi=-1}\sin\delta_s\cdot\cos\delta_s\\ &= q_{i,n}\sin\delta_s\\ &= (q_{0,n}-\dot{m}h_v)\cdot\sin\delta_s.\end{aligned} \tag{3.7}$$

For general materials, the ablation rate ($\dot{m}$) in thermal equilibrium depends on the surface temperature and the local pressure. The discussion concerning this problem will be made in the latter section.

3.2.2. *Boundary Conditions on the Interface between the Solid Layer and the Gel Layer*

At the interface between the solid layer and the gel layer, the temperature must be continuous, that is

$$T_1 = T_m = T_2. \tag{3.8}$$

On the other hand heat flux balance across the interface ($\chi=0$ or $\xi=0$) may be expressed as

$$\begin{aligned} &-k_1 \frac{\partial T_1}{\partial x} \sin\delta_i + k_1 \frac{\partial T_1}{\partial r} \cos\delta_i - \rho_2 \cdot h_m \cdot (\dot{s}+\dot{\theta}) \sin\delta_i \\ &\quad = -k_2 \frac{\partial T_2}{\partial x} \sin\delta_i + k_2 \frac{\partial T_2}{\partial r} \cos\delta_i, \end{aligned} \tag{3.9}$$

where h_m is the latent heat for phase change from the solid to the gel, and δ_i is the angle the local interface in the meridian plane makes with the axis of symmetry.

Furthermore, the following expression may be obtained from the geometrical relation at the interface ($\chi=0$)

$$\begin{aligned} \cot\delta_i &= -\frac{\partial L}{\partial r} \\ &= -\frac{\partial}{\partial r}(L_0 - x_i - s - \theta) \\ &= A - \frac{dL_0}{dr}. \end{aligned} \tag{3.10}$$

With this equation together with Eq. (2.3), Eq. (3.9) can be rewritten as

$$\begin{aligned} &-\left(\frac{k_1}{\theta}\frac{\partial T_1}{\partial \chi}\right)_{\chi=0} \sin\delta_i + k_1 \cdot \cos\delta_i \left(\frac{\partial T_1}{\partial r} - \frac{A}{\theta}\frac{\partial T_1}{\partial \chi}\right)_{\chi=0} \\ &\quad -\rho_2 \cdot h_m \cdot (\dot{s}+\dot{\theta}) \cdot \sin\delta_i \\ &= -\left(\frac{k_2}{\theta}\frac{\partial T_2}{\partial \chi}\right)_{\chi=0} \sin\delta_i + k_2 \cdot \cos\delta_i \left(\frac{\partial T_2}{\partial r} - \frac{A}{\theta}\frac{\partial T_2}{\partial \chi}\right)_{\chi=0}, \end{aligned} \tag{3.11}$$

where k_2 is the thermal conductivity in the solid layer.

3.2.3. *Boundary Conditions on the Backface*

In the present approach it is assumed that the backface is thermally insulated, that is

$$\frac{\partial T(r, 1, t)}{\partial \xi} = 0. \tag{3.12}$$

3.2.4. *Boundary Conditions on the Centerline*

In the axisymmetric case under consideration an additional condition must be satisfied along the axis of symmetry, which may be expressed as

$$\frac{\partial T(0, \chi, t)}{\partial r} = 0, \qquad -1 \leq \chi \leq 0 \tag{3.13}$$

and

$$\frac{\partial T(0,\xi,t)}{\partial r}=0, \qquad 0\leq\xi\leq 1. \tag{3.14}$$

3.3. Local Heat-Transfer Rates and Free-Stream Conditions

Since the local ablation rate is dependent on time and location, the body shape changes with time. This, in turn, leads to the change in boundary layer flow on the body surface and, consequently, in local heating rate. However, from the quasi-steady assumption of boundary layer flow, this effect may be reasonably involved in the steady state heating rate q_0 proposed by Lees [*16*], if it is evaluated under the instantaneous boundary conditions.

On the other hand, a small amount of mass is injected into the boundary layer flow due to ablation, so that the heat transfer rate to the wall may be reduced. Because of this, q_0 must be modified by taking the effect of mass addition into account in the present approach. For this purpose, a mass addition parameter B is to be introduced which is defined by the equation

$$B=\frac{\rho_w v_w}{\rho_\infty u_\infty St}, \tag{3.15}$$

where $\rho_w v_w$ denotes the rate of mass addition and St is the Stanton number defined as

$$St=\frac{q_{w,B=0}}{(H_{st}-H_w)\rho_\infty u_\infty}, \tag{3.16}$$

where H is total enthalpy and subscript w indicates wall conditions.

The physical meaning of the mass-addition parameter B is the ratio of injected mass rate to the fraction of the maximum available heat arriving at the surface without mass addition. Thus, by use of Eq. (3.16), Eq. (3.15) can be rewritten as

$$B=\dot{m}\frac{H_{st}-H_w}{q_{w,B=0}}. \tag{3.17}$$

As to the stagnation flow, many studies ([*2*], [*3*], [*17*], [*18*]) have been conducted on reduction of heat transfer rate due to mass addition and it is shown that the effect of mass addition can be formulated as a function of mass addition parameter only. Based on these theoretical informations, Marvin and Pope [*3*] reviewed entire problems and proposed a simple relation between heating rate and mass addition parameter such as

$$\begin{aligned}\Psi&=\frac{q_B}{q_{B=0}}=\Psi(B)\\&=1-0.72\left(\frac{M_{\text{air}}}{M_{\text{Teflon}}}\right)^{0.25}B+0.13\left(\frac{M_{\text{air}}}{M_{\text{Teflon}}}\right)^{0.5}B^2,\end{aligned} \tag{3.18}$$

where M_{air} and M_{Teflon} are the molecular weight, and showed that this relation can predict experimental results fairly well in many cases.

As has been just mentioned above, Eq. (3.18) is valid only in the stagnation region. Moreover, it must be noted that the boundary layer flow downstream of the point of injection will be influenced by the injected mass and, consequently, this turns out a modification of the local heating rate there. However, considering that the downstream influence of the added mass is dependent on the mass flow rate of the injection, it may be deduced that the injected mass has a primary effect on reduction of the heating rate just at the point of injection while it has a secondary effect on the local heat transfer rate downstream, although there is no rigorous proof for this statement.

Because of this and also because there does not seem to exist any other conventional method available to estimate local heating rate with mass injection over the entire surface, in the present approach is introduced an additional simple assumption that the modification denoted by Eq. (3.18) may be applicable everywhere on the ablating surface.

A rough evaluation reveals that the ablation rate obtainable within the range of the present development is of the order of $10^{-3}\,\mathrm{gr}\cdot\mathrm{cm}^{-2}\cdot\mathrm{sec}^{-1}$. From this fact together with the results presented by Swann et al. [*19*], Rubesin et al. [*20*], etc., it may be expected that this assumption is valid.

Since the body shape changes with time, the external inviscid flow outside the boundary layer also changes with time. For simplicity, it is assumed that the external flow conditions can be given by the modified Newtonian theory, which has been proved to be sufficiently accurate for most applications where the body is spherically blunted.

4. Relation between the Wall Temperature T_w and the Ablation Rate $\dot{m}$

Ablation under consideration is a very complicated phenomenon associated with coupling of a nonequilibrium chemical process with an aerodynamic one and, therefore, it may be of a primary interest to clarify the mechanism for determining the ablating field.

Since ablation rate $\dot{m}$ (mass loss rate of solid material per unit surface area and unit time), which is one of the most characteristic quantities for predicting the ablation phenomenon, is essentially a kind of chemical reaction rates, it can be considered to be expressed in terms of two thermodynamic variables (wall temperature T_w and pressure p) of state in a form

$$\begin{aligned}\dot{m} &= (\rho v)_w \\ &= F(T_w, p),\end{aligned} \tag{4.1}$$

where a functional form F may be determined from chemical kinetics. It must be noted that Eq. (4.1) includes substantial characteristics of solid material implicitly and may be considered to give a static relation necessary for all the fields where ablation occurs.

However, it is evident from many experiments and data [*21*], [*22*] that the pressure dependence of ablation rate is negliglble in the range of low surface temperature.

This static relation between $\dot{m}$ and T_w for Teflon has already been proposed by Rashis and Hopko [*23*] such as shown in Fig. 3. In the present approach the curve presented in Fig. 3 is approximated by the following expression,

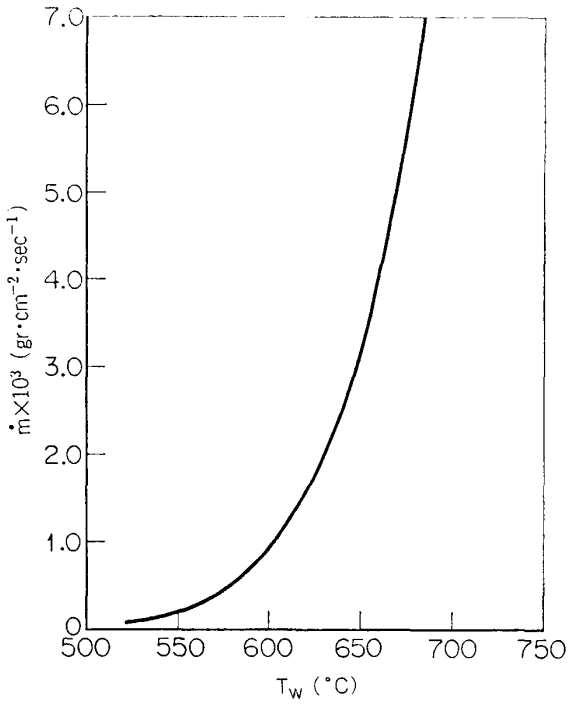

FIG. 3. Static Relation between $\dot{m}$ and T_w for Teflon.

$$\begin{aligned}\dot{m} &= \rho_1 \frac{\partial s}{\partial t} \sin \delta_s \\ &= \exp\,(aT_w^2 + bT_w + c),\end{aligned} \tag{4.2}$$

where a, b and c are constants.

In Ref. *24* it is pointed out that the range of applicability of Eq. (4.2) is $p<1$ atm and $T_w<800°C$. Therefore, the present approach must be restricted within this range.

5. Numerical Calculations

5.1. Singularity along the Axis of Symmetry

Eqs. (2.4) and (2.7) are applied to the entire region of interest. It is clear from direct examination of these equations that, along the axis of symmetry ($r=0$), there appears a singularity due to the term involving $1/r$. However, this singularity can be eliminated by considering the asymptotic behavior as r tends to vanish. Examination of the terms reveals that the numerator tends to vanish as the denominator approaches zero, thus indicating the existence of a finite limit.

Application of L'Hospital's rule to this term gives

$$\lim_{r\to 0}\frac{\partial T/\partial r}{r}=\frac{\partial^2 T}{\partial r^2}\qquad \text{etc.} \tag{5.1.1}$$

Therefore, the heat conduction equation in the gel layer may be expressed along the axis of symmetry as

$$\frac{\partial T}{\partial t}=2\alpha\frac{\partial^2 T}{\partial r^2}+\frac{\alpha}{\theta^2}\frac{\partial^2 T}{\partial \chi^2}+\frac{1}{\theta}\frac{\partial T}{\partial \chi}\left\{\frac{\partial s}{\partial t}+(\chi+1)\frac{\partial \theta}{\partial t}-2\alpha\frac{\partial A}{\partial r}\right\}, \tag{5.1.2}$$

while in the solid layer it may be expressed as

$$\begin{aligned}\frac{\partial T}{\partial t}=&2\alpha\frac{\partial^2 T}{\partial r^2}+\frac{\alpha}{L^2}\frac{\partial^2 T}{\partial \xi^2}\\&+\frac{\partial T}{\partial \xi}\left\{2\alpha\xi\left(\frac{1}{\theta}\frac{\partial^2\theta}{\partial r^2}-\frac{1}{L}\frac{\partial^2 L}{\partial r^2}\right)\right.\\&\left.+\frac{1-\xi}{L}\left(\frac{\partial s}{\partial t}+\frac{\partial \theta}{\partial t}\right)-\frac{2\alpha}{L}\frac{\partial A'}{\partial r}\right\}.\end{aligned} \tag{5.1.3}$$

5.2. *Method of Solution*

The differential equations that predict temperature field in an ablating axisymmetric body of revolution has been presented in the previous section. In order to obtain a numerical solution to Eqs. (2.4) and (2.7), the differential equations must be approximated by finite-difference equations and programed for numerical computation by use of a high-speed digital computer.

In the present approach the numerical integration was carried out by use of the alternating-direction implicit (A. D. I.) method which has the advantages of being implicit, stable, and amenable to obtain rapid convergence of the solution.

A. D. I. method was first proposed by Peaceman and Rachford [25]. In this method, the second derivative $\partial^2 T/\partial r^2$ and the first derivative $\partial T/\partial r$ are replaced by a difference evaluated in terms of the unknown temperature at the time $t+\Delta t$, while the other derivatives, $\partial^2 T/\partial \chi^2$ and $\partial T/\partial \chi$, are replaced by a difference evaluated in terms of known temperatures at the time t. This formulation is implicit in the r-direction. The procedure is then repeated for the second time step of equal size, with the formulation implicit in the χ-direction and, thus, the alternation in solution, that is, column-row, is continued over the specified time period.

It must be noted that a pair of successive row-column integrations is required to maintain a stable numerical solution. Moreover, the successive pairs of the integrations must have in general the same time step. In other words, this method is unstable in each time step so that the formulation only in one direction must not be used due to the large growth of errors. Thus, when solved alternately, this method is valid for all ratios of $\Delta t/(\Delta \chi)^2$ and $\Delta t/(\Delta r)^2$. Unfortunately, a comprehensive explanation can not be made yet on the conditions of its validity.

Since Eqs. (2.4) and (2.7) consist of the first, the second and the cross derivatives, these derivatives are replaced, respectively, by finite-difference forms throu gh

Taylor's series expansions, where forward, central and backward differences are employed. All derivatives are evaluated to the accuracy of the order of $\Delta\chi^2$ or Δr^2.

The finite-difference equations thus obtained have the form, for either a row or a column solution, as

$$A_i T_{i-1} + B_i T_i + C_i T_{i+1} = D_i, \tag{5.2.1}$$

where $i=1, 2, \cdots, L+1$ are for the column solution and $i=1, 2, \cdots, M+1$ for the row solution. Eq. (5.2.1) represents a set of $L+1$ or $M+1$ equations with $L+1$ or $M+1$ unknown temperatures. Since Eq. (5.2.1) results in a tridiagonal matrix of unknown temperatures, this set of equations can be easily solved.

5.3. Numerical Calculations

The Eqs. (2.4) and (2.7) are solved under the initial and boundary conditions by use of the finite-difference method mentioned in the last section.

Wentink [*24*], Siegle et al. [*26*], Friedman [*27*] etc. studied physical properties of Teflon and obtained slightly different results, respectively. In the present approach, the mean values are, therefore, used in numerical calculations.

Free stream conditions, models, and physical properties used in calculations are as follows;

$M_\infty = 5.74$, $p_{st} = 1$ atm, $T_{st} = 900$—$1200°C$,
$R_b = 1$ cm, $L_0 = 2.5$ cm, $T_m = 327°C$,
$k_1 = 2.00 \times 10^{-4}$ cal·cm^{-1}·s^{-1}·deg^{-1},
$k_2 = 6.00 \times 10^{-4}$ cal·cm^{-1}·s^{-1}·deg^{-1},
$\alpha_1 = 4.02 \times 10^{-4}$ cm^2·s^{-1},
$\alpha_2 = 1.19 \times 10^{-3}$ cm^2·s^{-1},
$\rho_1 = 1.72$ gr·cm^{-3},
$\rho_2 = 2.10$ gr·cm^{-3},
$h_v = 370$ cal·gr^{-1}, $h_m = 14$ cal·gr^{-1}.

Numerical procedure may summarized as follows;

(1) A prescribed initial temperature profile T_i is smaller than T_m (that is, $T_i < T_m$), so that the gel layer does not exist initially. For this reason, a heat conduction equation for a single-layer material is first solved until the phase transition temperature T_m is reached at the surface.

(2) After the surface temperature has risen up to the phase transition temperature T_m, heat conduction equations for a two-layer material are solved by use of its temperature distribution as an initial conduction.

(3) The calculation is continued over the specified time period.

6. Results and Discussions

6.1. Experiment

6.1.1. Wind Tunnel and Models

The experiment was carried by use of a high enthalpy hypersonic wind tunnel, which consists of a high temperature air-supply system, the wind tunnel system, and an exhaust system. A diagram of the facility systems is shown in Fig. 4. The free stream conditions used in the present experiment are as follows;

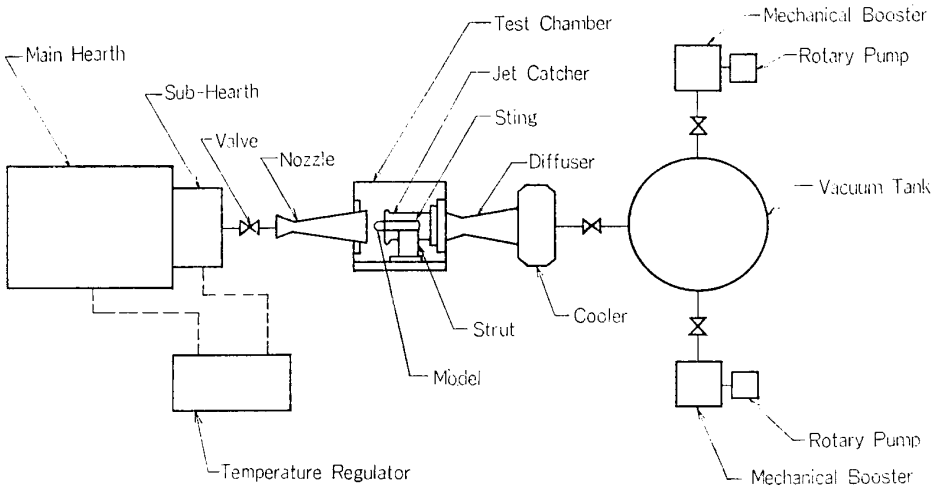

Fig. 4. Diagram of the Experimental Facility Systems.

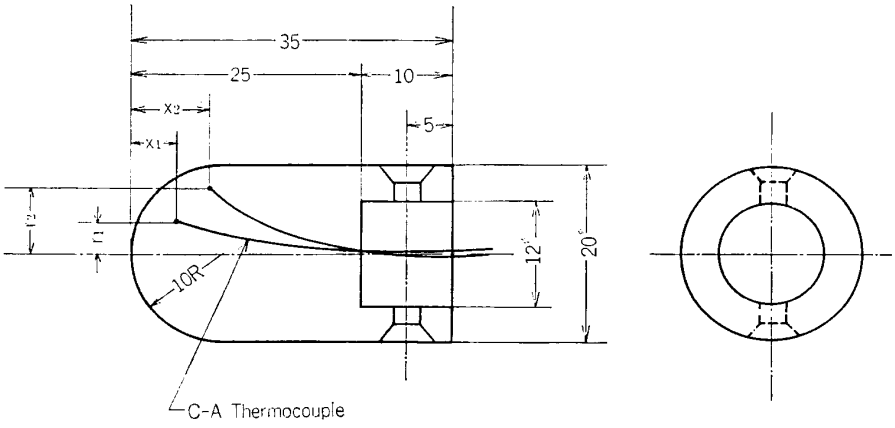

Fig. 5. Model.

Mach number	$M_\infty = 5.74$,
stagnation temperature	$T_{st} = 1020°C$,
stagnation pressure	$p_{st} = 1$ atm.

Hemisphere-cylinder models made of Teflon were used in the experiment, the size of which is shown in Fig. 5 in detail.

As a temperature sensor was used a $C-A$ thermocouple, each element of which is 0.1 mm ϕ in diameter. Since it was too difficult to put a number of sensors in

a model, either one or several thermocouples were burried in each model. Soft-X ray photographs (see Fig. 6) were used to check the state of the burried thermocouples and the position of their junction.

6.1.2. Measurements

Measurements were made on instantaneous internal temperature distributions and the recession depth (s). In this experiment, the origin of the time-axis is taken at the time when the valve of the wind tunnel is opened. Instantaneous shapes of an ablating model are measured by use of photographs which were taken at intervals

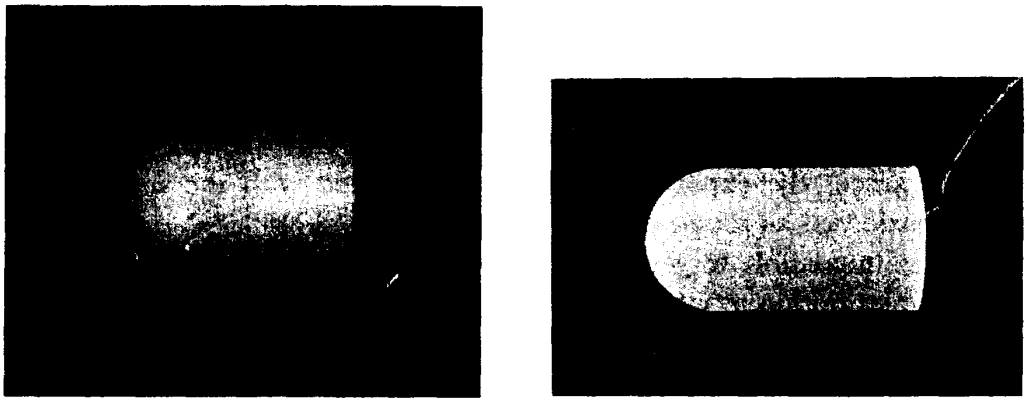

Soft-X ray photograph Model

FIG. 6. Soft-X Ray Photograph.

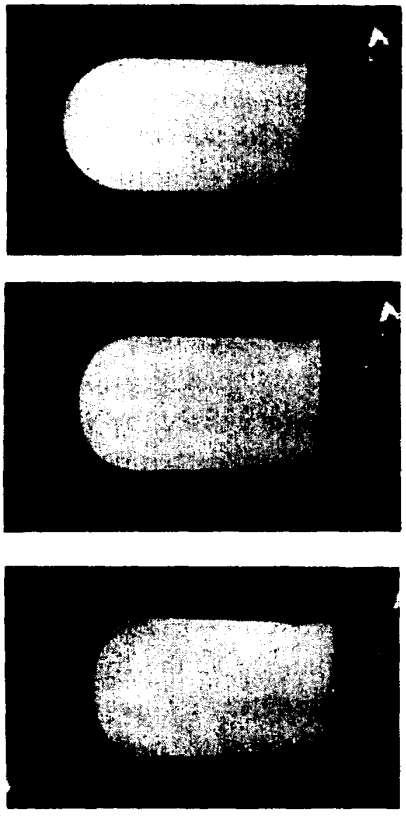

$t=0$ sec.

$t=40$ sec.

$t=80$ sec.

FIG. 7. Typical Photographs of an Ablating Model.

of ten seconds. To indicate the instantaneous body shape, orthogonal coordinates (r, x) (see Fig. 1) are used.

Typical photographs of an ablating model are showed in Fig. 7. However, it must be remarked that these photographs do not indicate a true recession depth $s(r, t)$ but an apparent one involving thermal expansion of the body. Because of this, the apparent recession depth measured from the photographs must be modified by subtracting the effect of thermal expansion to obtain the true recession depth. In the present experiment, the effect of the thermal expansion was estimated in such a way that displacements of the marks, which had been marked before wind tunnel operation at several positions along a meridian line of the model, were measured from the photographs and the displacement of the ablating surface due to thermal expansion was evaluated approximately by extrapolation of these data.

Within the range of the present experiment, the thermal expansion thus estimated was small but the same order of magnitude compared with the true recession depth and, in this sense, the experimental results associated with the surface recession should be considered as rough evaluation.

Since it was impossible to get data at many points simultaneously in a model, the temperature distribution at any time was obtained by superposition of the temperature histories measured at several different points in each case of the experiment. Of course, for this purpose the validity of the superposition had been confirmed by checking reproducibility of the experimental data [*28*].

6.2. *Numerical Results and Discussions*

With an emphasis laid on the effect of the gel layer on internal temperature distributions, numerical calculations were carried out for the same hemisphere model made of Teflon as used in the experiment, where the stagnation temperature in the free stream was taken as a parameter. The size of the model is shown in Fig. 5.

In Figs. 8 and 9 is presented the variation of normal recession depth of the surface with time at $r=0$ mm (stagnation point) and $r=6.0$ mm, respectively. It is remarkable that the rate of surface recession clearly tends to reach a constant value in a short time, resulting in that the steady ablation may be attained apparently. To clarify this in more detail the variation with time of the surface temperature and the growth of thickness of the gel layer at the stagnation point are shown in Fig. 10, where the overshoot of each curve may be caused by the error in numerical computation. As is seen in this figure, the surface temperature goes rapidly up to the second order transition temperature, beyond which it further continues to rise more rapidly because of the significant decrease of thermal diffusivity near the surface due to growth of the gel layer.

The surface temperature finally reaches a constant values in a short time, beyond which it seems to be kept almost unchanged as the time goes on, indicating that the ablation rate attains to the steady state value. This characteristic in transient wall temperature is consistent with that of the surface recession rate.

On the other hand, the gel layer, which begins to grow very rapidly at the time the second order transition is approached, still continues to grow after the surface

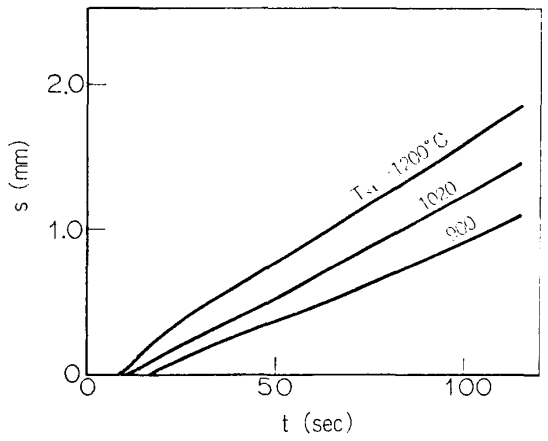

FIG. 8. History of Normal Recession Depth of Ablating Surface.
$M_\infty=5.74$, $p_{st}=1$ atm, $r=0$ mm.

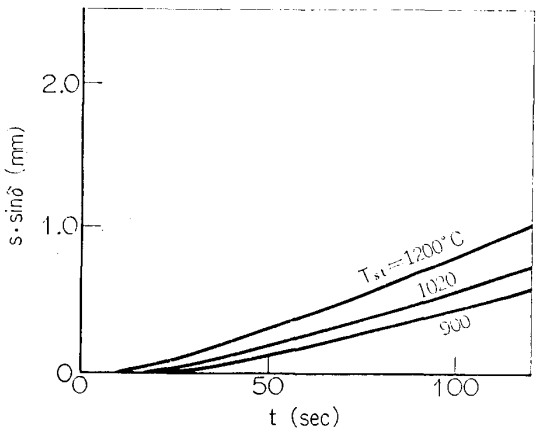

FIG. 9. History of Normal Recession Depth of Ablating Surface.
$M_\infty=5.74$, $p_{st}=1$ atm, $r=6.0$ mm.

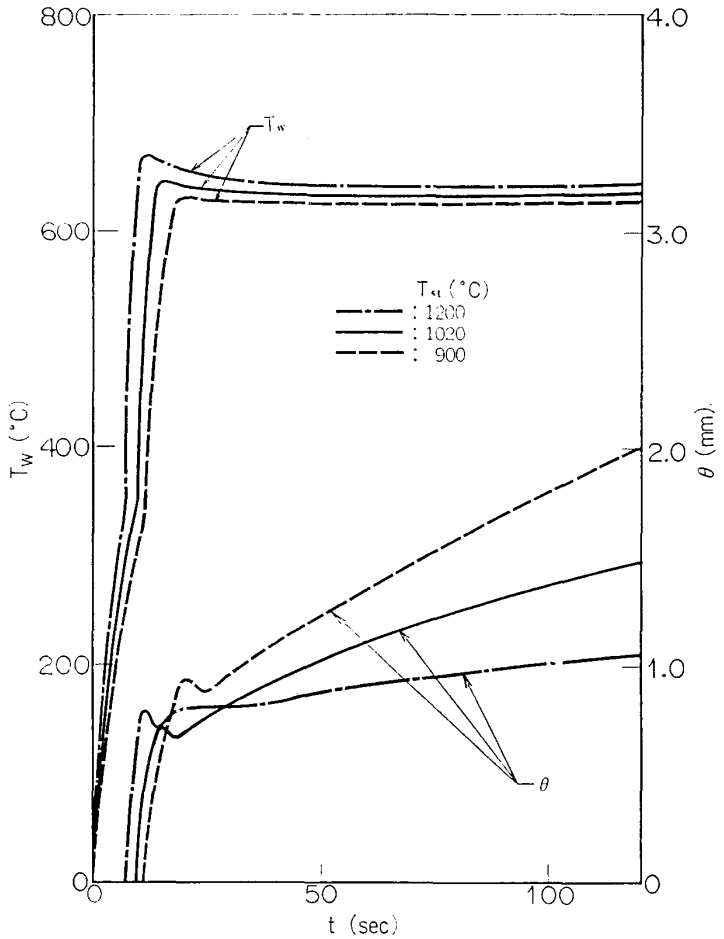

FIG. 10. Surface Temperature and Thickness of Gel Layer at Stagnation Point.
$M_\infty=5.74$, $p_{st}=1$ atm.

temperature has attained to the steady state, although the rate of its growth may decrease considerably. This suggests implicitly that the temperature in the body

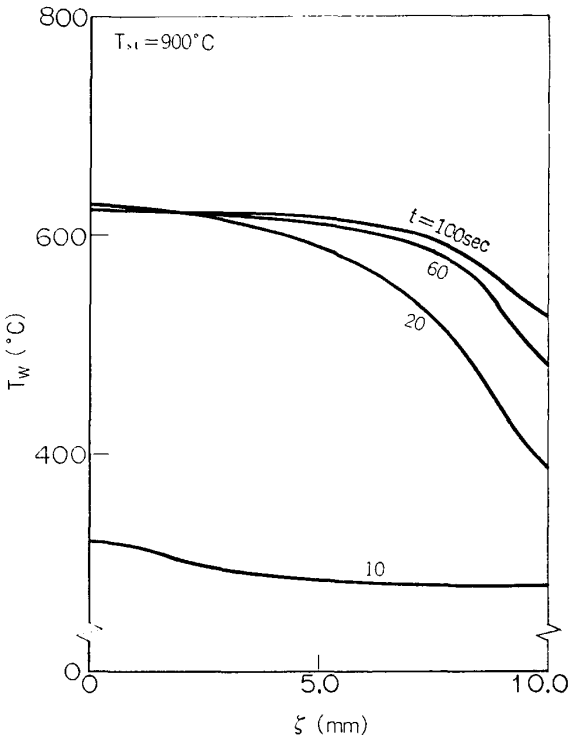

FIG. 11(a)

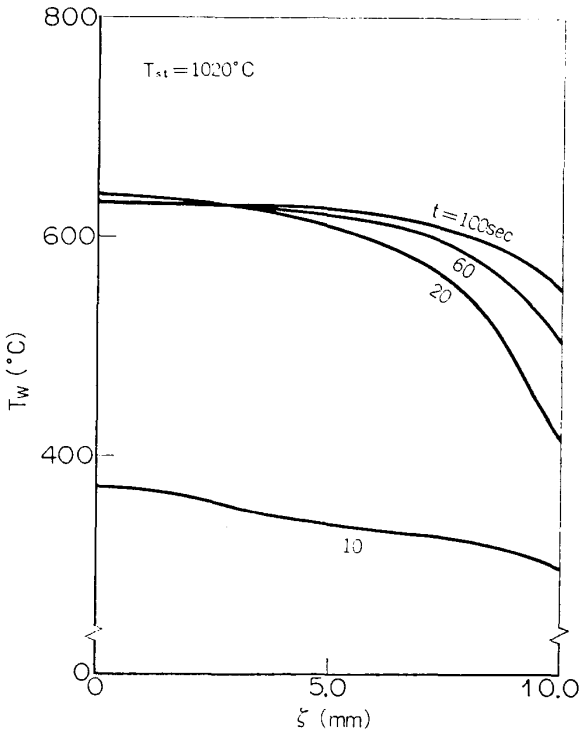

FIG. 11(b)

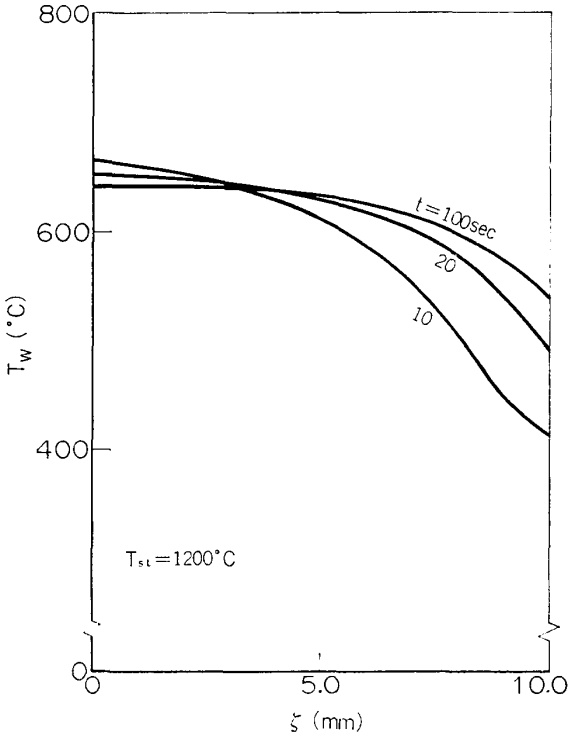

FIG. 11(c)

FIG. 11(a). Instantaneous Distribution of Surface Temperature.
M_∞=5.74, p_{st}=1 atm, T_{st}=900°C.

FIG. 11(b). Instantaneous Distribution of Surface Temperature.
M_∞=5.74, p_{st}=1 atm, T_{st}=1020°C.

FIG. 11(c). Instantaneous Distribution of Surface Temperature.
M_∞=5.74, p_{st}=1 atm, T_{st}=1200°C.

is still varing with time. Because of this it may be deduced that the assumption of the steady ablation is doubtful in its validity.

Figs. 11(a) to 11(c) show the instantaneous distribution of the surface tempera-

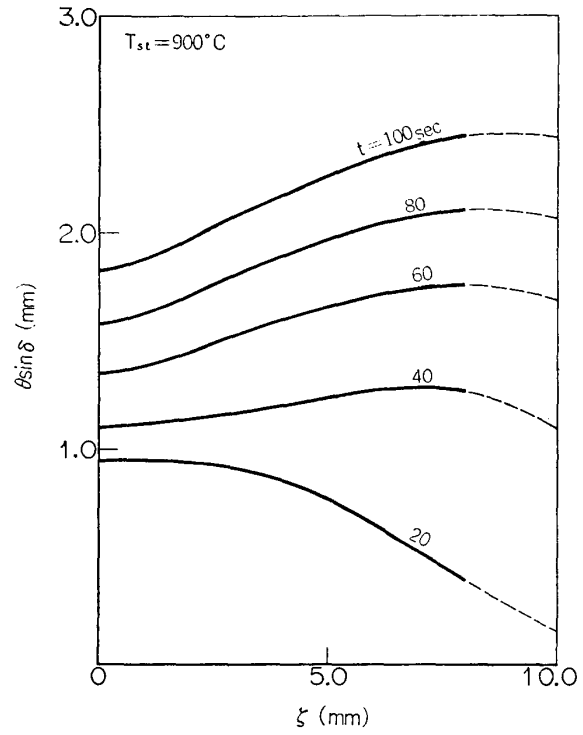

FIG. 12(a)

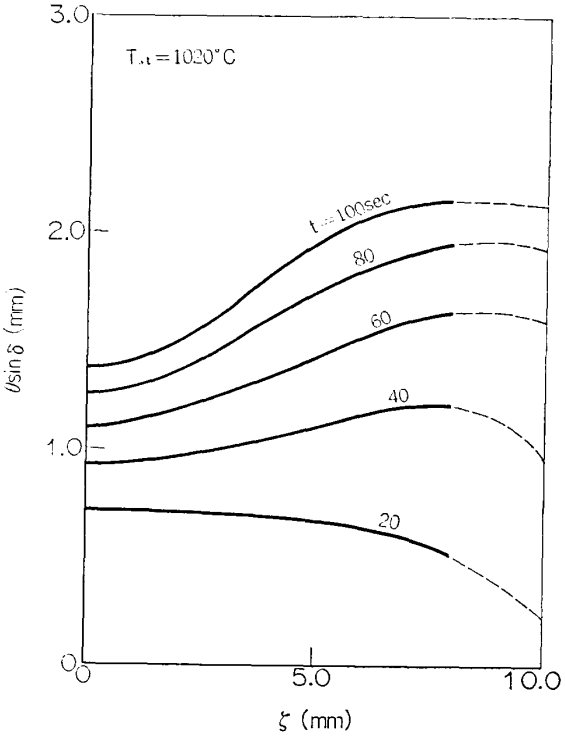

FIG. 12(b)

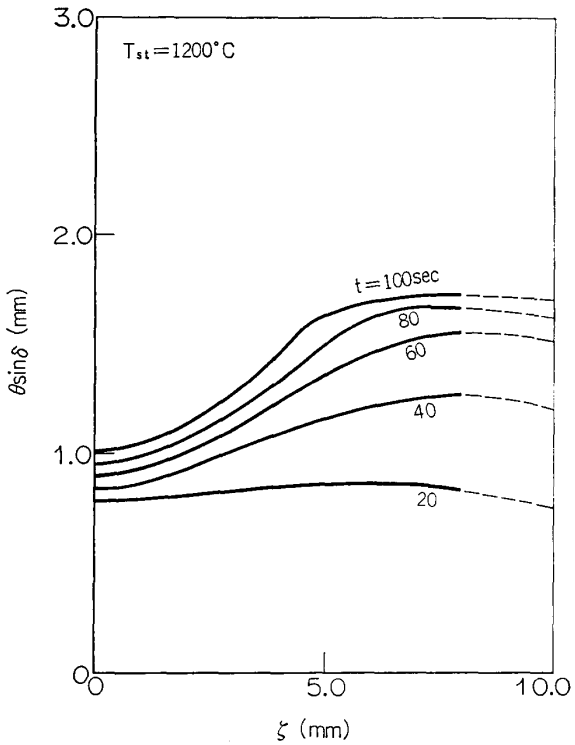

FIG. 12(c)

FIG. 12(a). Instantaneous Distribution of Normal Thickness of Gel Layer. $M_\infty=5.74$, $p_{st}=1$ atm, $T_{st}=900°C$.

FIG. 12(b). Instantaneous Distribution of Normal Thickness of Gel Layer. $M_\infty=5.74$, $p_{st}=1$ atm, $T_{st}=1020°C$.

FIG. 12(c). Instantaneous Distribution of Normal Thickness of Gel Layer. $M_\infty=5.74$, $p_{st}=1$ atm, $T_{st}=1200°C$.

ture, where ζ denotes the distance measured along a meridian line from the stagnation point. These figures clearly indicate the fact that the surface temperature near the stagnation point approaches the steady state very rapidly while it is still going

up at $t=100$ sec. in the region far downstream of the stagnation point. It is suggested from these results that the body is still changing its shape even at $t=100$ sec., resulting in the growth of the nose radius of curvature with time.

In Figs. 12(a) to 12(c) is presented the instantaneous distribution of normal thickness of the gel layer, where $\theta \sin \delta$ denotes the thickness normal to the ablating surface. It is clear from these results that the thickness of the gel layer decreases as the surface temperature increases, since the growth of the gel layer depends on the difference between the thermal diffusion velocity and the surface recession rate which increases very sensitively to a small increase in surface temperature.

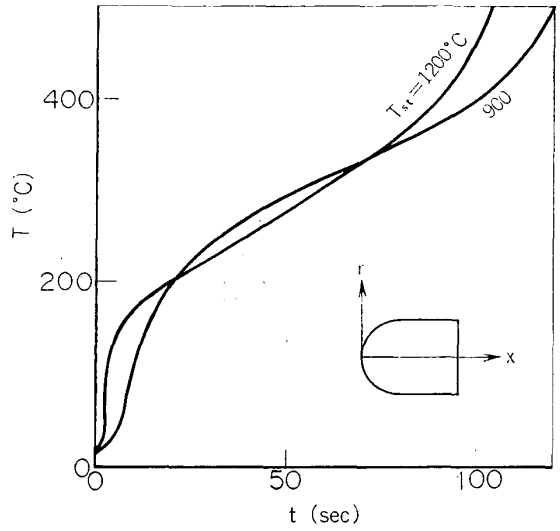

FIG. 13(a). Temperature History at $x=2.0$ mm and $r=0$ mm (centerline). $M_\infty=5.74$, $p_{st}=1$ atm.

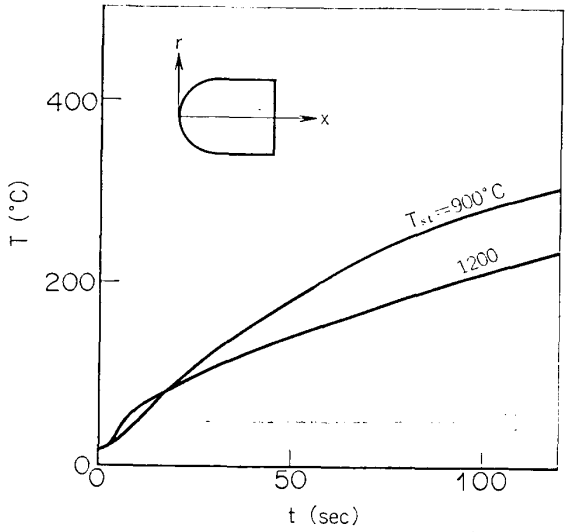

FIG. 13(b). Temperature History at $x=4.0$ mm and $r=0$ mm (centerline). $M_\infty=5.74$, $p_{st}=1$ atm.

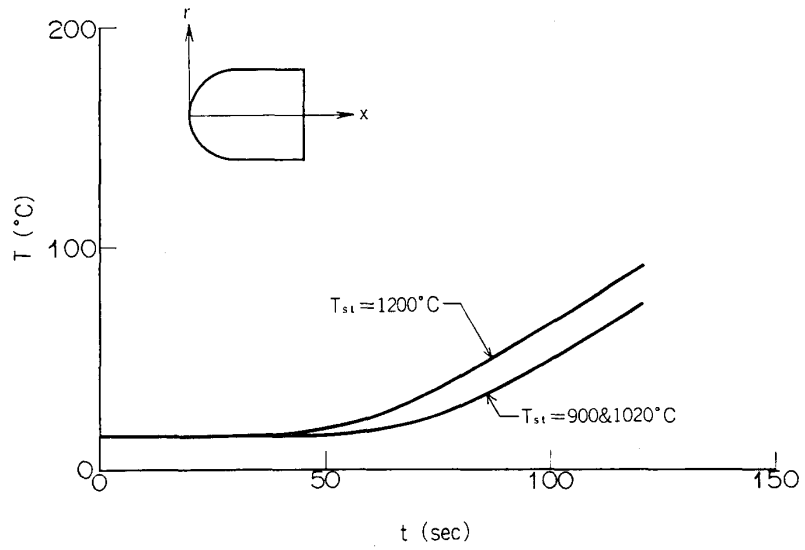

FIG. 13(c). Temparature History at $x=25.0$ mm (backface) and $r=0$ mm (centerline). $M_\infty=5.74$, $p_{st}=1$ atm.

The temperature history in the body is another point of interest. Figs. 13(a) to 13(c) show the temperature history at several fixed points on the axis of symmetry, where the coordinates system (r, x) is fixed on the initial surface of the body. As is seen in Fig. 13(a), the temperature at the point locating close to the surface becomes temporarily lower for the main stream with higher enthalpy for the time from 20 sec. to 70 sec. This temporary reversal of the internal temperature seems to become predominant as the observed point goes further inside the body, as shown in Fig. 13(b), while it is no longer observed at the point locating far inside, as is seen in Fig. 13(c). This characteristic seems to be caused by the existence of the gel layer.

In Figs. 14(a) and 14(b) is presented the instantaneous distribution of temperature along the axis of symmetry. To demonstrate the effect of transverse conduction of heat the instantaneous distribution of temperature along the line $r=6.0$ mm is shown in Figs. 15(a) and 15(b) for comparison. These figures clearly indicate a remarkable fact that, except in the region very close to the surface, the transverse heat conduction has a significant effect to increase the local temperature other than on the axis of symmetry.

In order to demonstrate the effect of the gel layer on the transient thermal response the instantaneous temperature distribution along the axis of symmetry was calculated by use of the single layer model and the results are shown in Fig. 16 together with those of two layer model for comparison. Although the temperature profile with gel layer may be nearly similar to that without gel layer for an initial while, the discrepancy between these two profiles becomes increasingly remarkable,

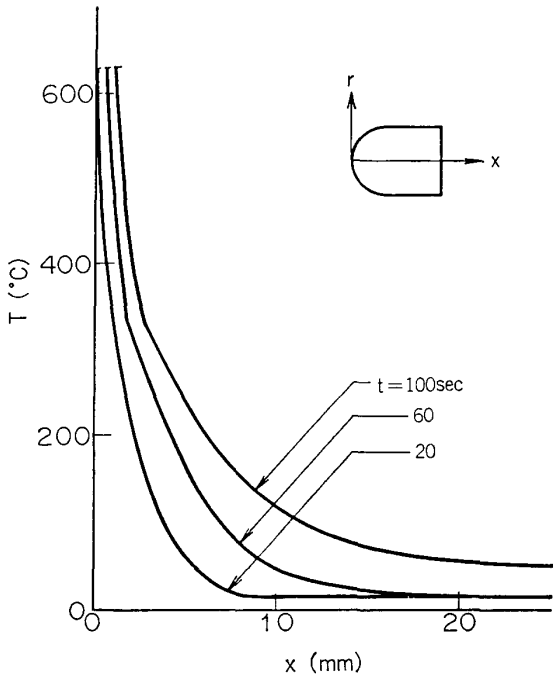

FIG. 14(a). Instantaneous Temperature Distribution along the Centerline. $M_\infty=5.74$, $p_{st}=1$ atm, $T_{st}=900°C$.

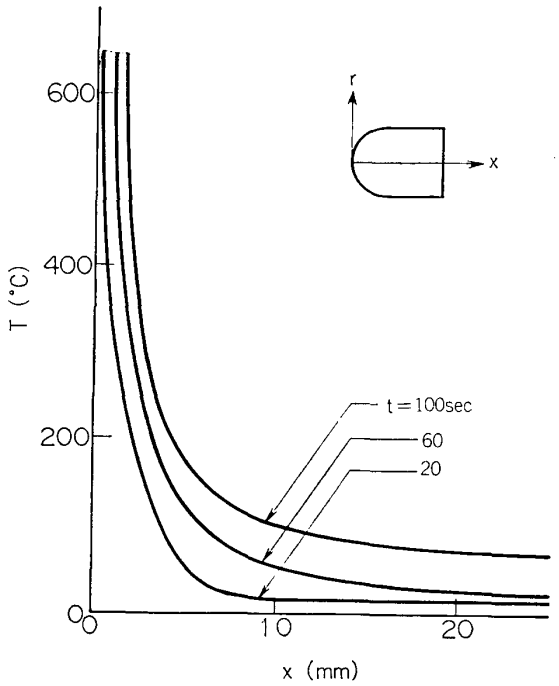

FIG. 14(b). Instantaneous Temperature Distribution along the Centerline. $M_\infty=5.74$, $p_{st}=1$ atm, $T_{st}=1200°C$.

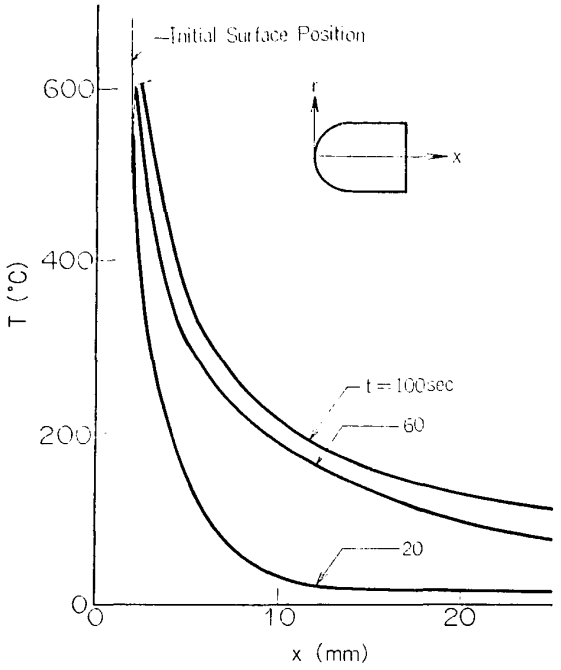

FIG. 15(a). Instantaneous Temperature Distribution at $r=6.0$ mm.
$M_\infty=5.74$, $p_{st}=1$ atm, $T_{st}=900°C$.

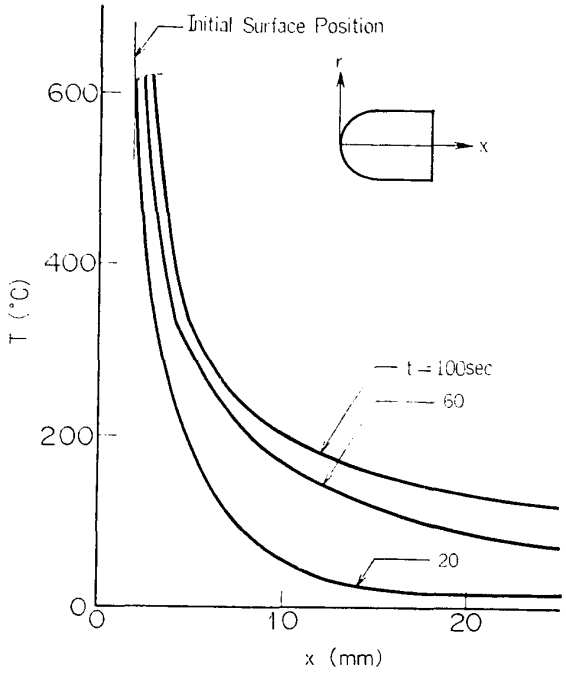

FIG. 15(b). Instantaneous Temperature Distribution at $r=6.0$ mm.
$M_\infty=5.74$, $p_{st}=1$ atm, $T_{st}=1200°C$.

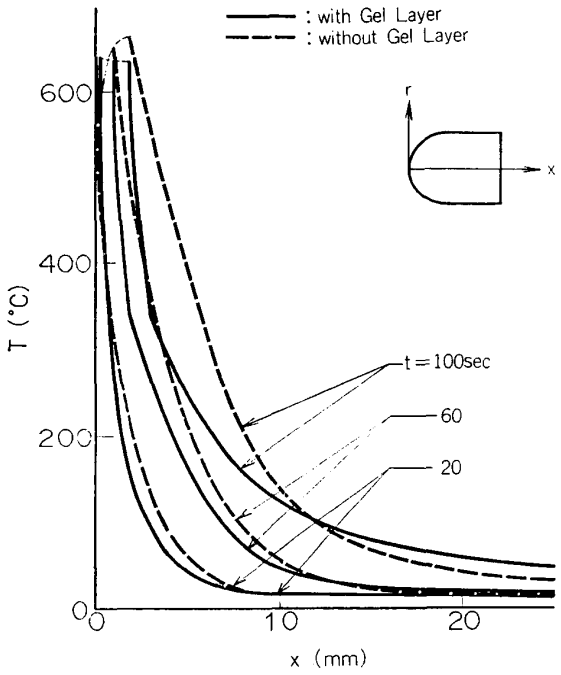

FIG. 16. Instantaneous Temperature Distribution along the Centerline.
$M_\infty=5.74$, $p_{st}=1$ atm, $T_{st}=1020°C$.

indicating that the single layer model gives significant higher temperature near the surface than the two layer model.

Another important factor for evaluation of effectiveness of the gel layer is the thermal thickness, which is a function of time in the transient analysis. Since the thermal thickness is a characteristic length representing the effective range of

thermal diffusion, the small thickness may be considered to correspond roughly to a steep descent in temperature near the surface due to the gel layer and, consequently, to the effective heat protection. In the present approach it is defined, for convenience' sake, by use of the instantaneous temperature distribution along the axis of symmetry at $t=100$ sec. as

$$\delta_{t=100}=\left(\frac{1}{T_w}\int_{x_i+s}^{L_0} T dx\right)_{\substack{t=100\\ r=0}}, \tag{6.1}$$

where x_i+s is the location of the stagnation point.

In Fig. 17 is presented the variation of thermal thickness with stagnation temperature in the main stream. As is seen in this figure, the thermal thickness decreases with increase of enthalpy in free stream. This, in turn, leads to the deduction that the effectiveness of the gel layer might be correlated to the time of

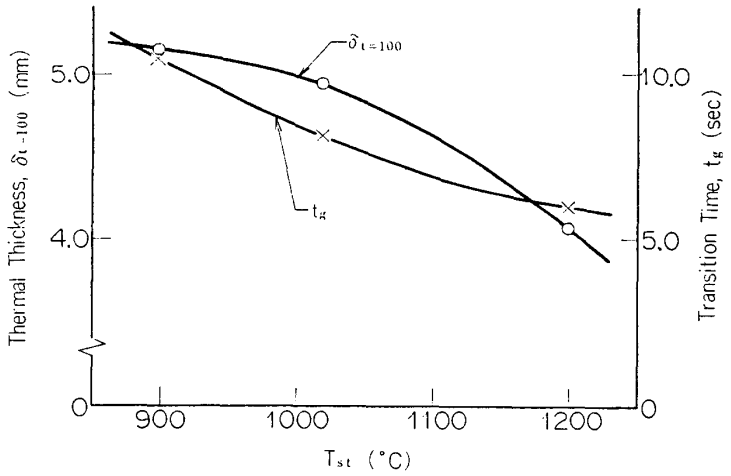

FIG. 17. Thermal Thickness $\delta_{t=100}$ and Transition Time t_g.

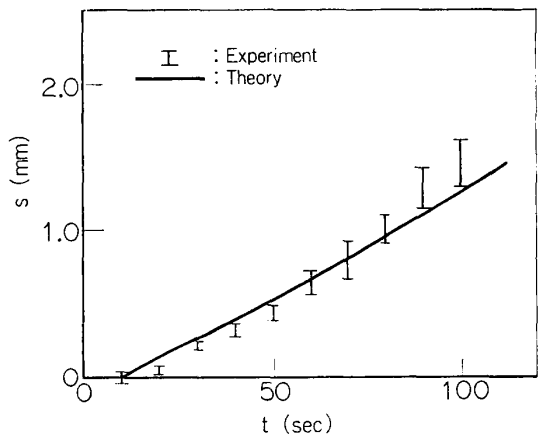

FIG. 18. History of Surface Recession at Stagnation Point.
$M_\infty=5.74$, $p_{st}=1$ atm, $T_{st}=1020$°C, $R_b=10.0$ mm.

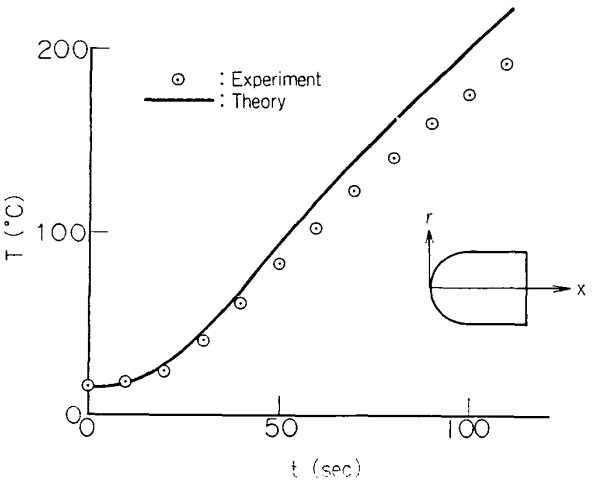

FIG. 19. Temperature History at $x=5.9$ mm and $r=0.6$ mm.
$M_\infty=5.74$, $p_{st}=1$ atm, $T_{st}=1020$°C, $R_b=10.0$ mm.

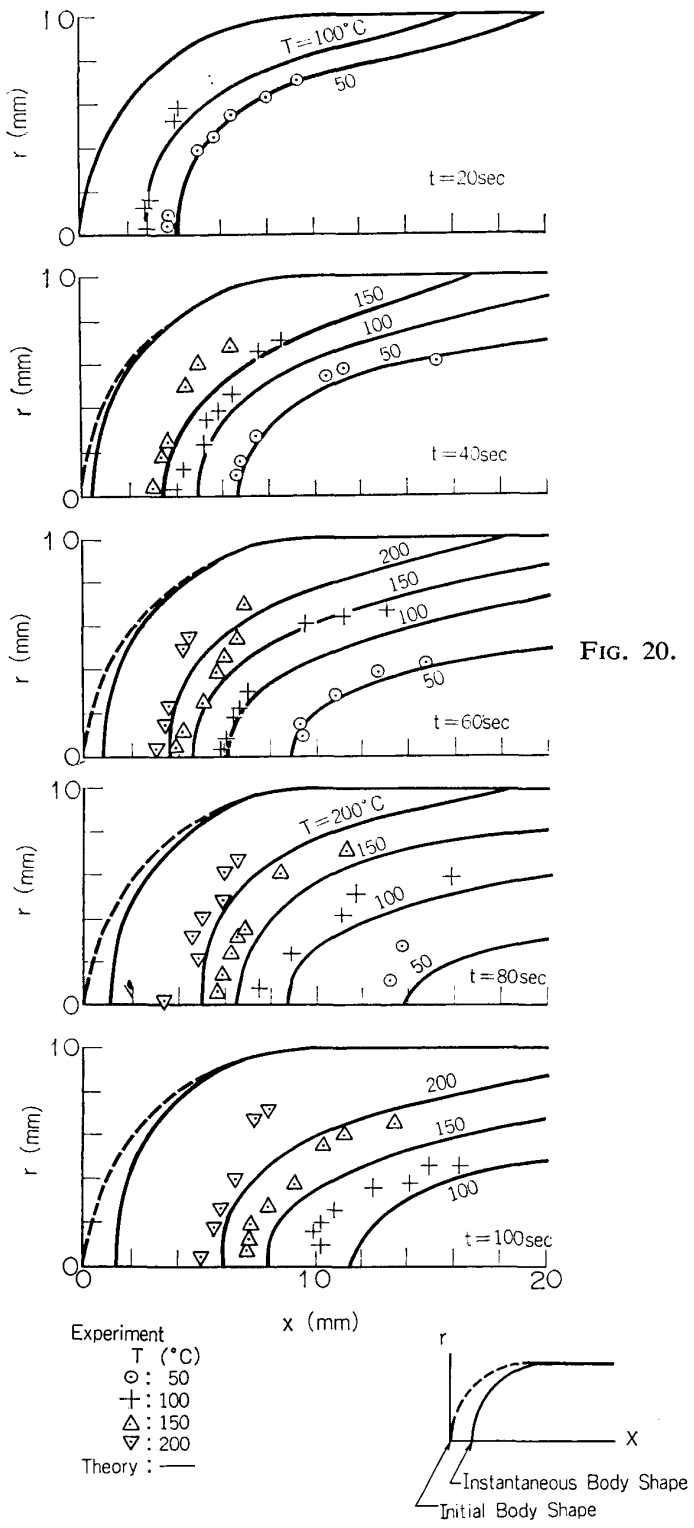

FIG. 20. Instantaneous Internal Temperature Distribution with Gel Layer. $M_\infty=5.74$, $p_{st}=1$ atm, $T_{st}=1020°C$.

appearance of the gel layer. In order to examine this in more detail, the transition time t_g that is defined as the time the second order transition first occurs at the stagnation point is also plotted in Fig. 17. The result clearly indicates the fact that the earlier the second order transition occurs, the more the effectiveness of the gel layer increases, thus confirming the deduction mentioned above.

Comparison of the numerical results with experimental ones is another point of interest. Fig. 18 shows the history of surface recession depth at the stagnation point. As has been already mentioned in Section 6.1., the true surface recession rates obtained in the experiment are dispersed inevitably due to the error in estimation of the effect of the thermal expansion. However, despite of this circumstance the agreement between the present theory and the experiment seems to be fairly good, as is seen in this figure.

In Fig. 19 is presented a comparison of the temperature history at a fixed point in the body. In the early period of time the agreement between theory and experiment is quite good, while the theory seems to deviate increasingly from the experiment as the time goes on. This may be caused by accumulation of error in the numerical computation.

Fig. 20 shows the theoretical results of the instantaneous isothermal lines calculated by use of the two layer model. The experimental results are also plotted in the same figure for comparison. It must be remarked in this figure that, in the early period of time, the present theory agrees well with the experiment not only qualitatively but also quantitatively. Moreover, although the quantitative difference between the theory and the experiment may increase due to accumulation of error in the numerical computation as the time proceeds, the qualitative agreement seems to be preserved fairly well. The same trend can be seen in the instantaneous temperature distribution along the axis of symmetry, as shown in Fig. 21. Therefore, these results seems to give an experimental evidence to the validity of the present approach.

In order further to demonstrate indirectly the validity of the two layer model, the numerical computation was carried out by use of the single layer model to obtain

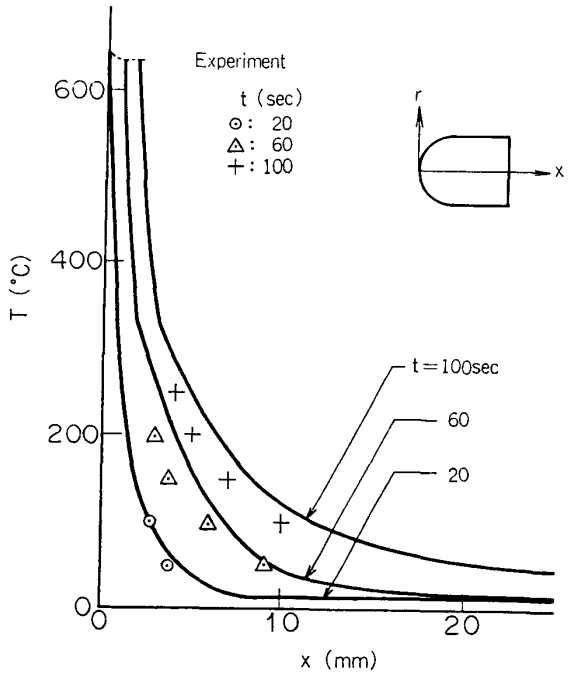

FIG. 21. Instantaneous Temperature Distribution along the Centerline.
$M_\infty=5.74$, $p_{st}=1$ atm, $T_{st}=1020°C$.

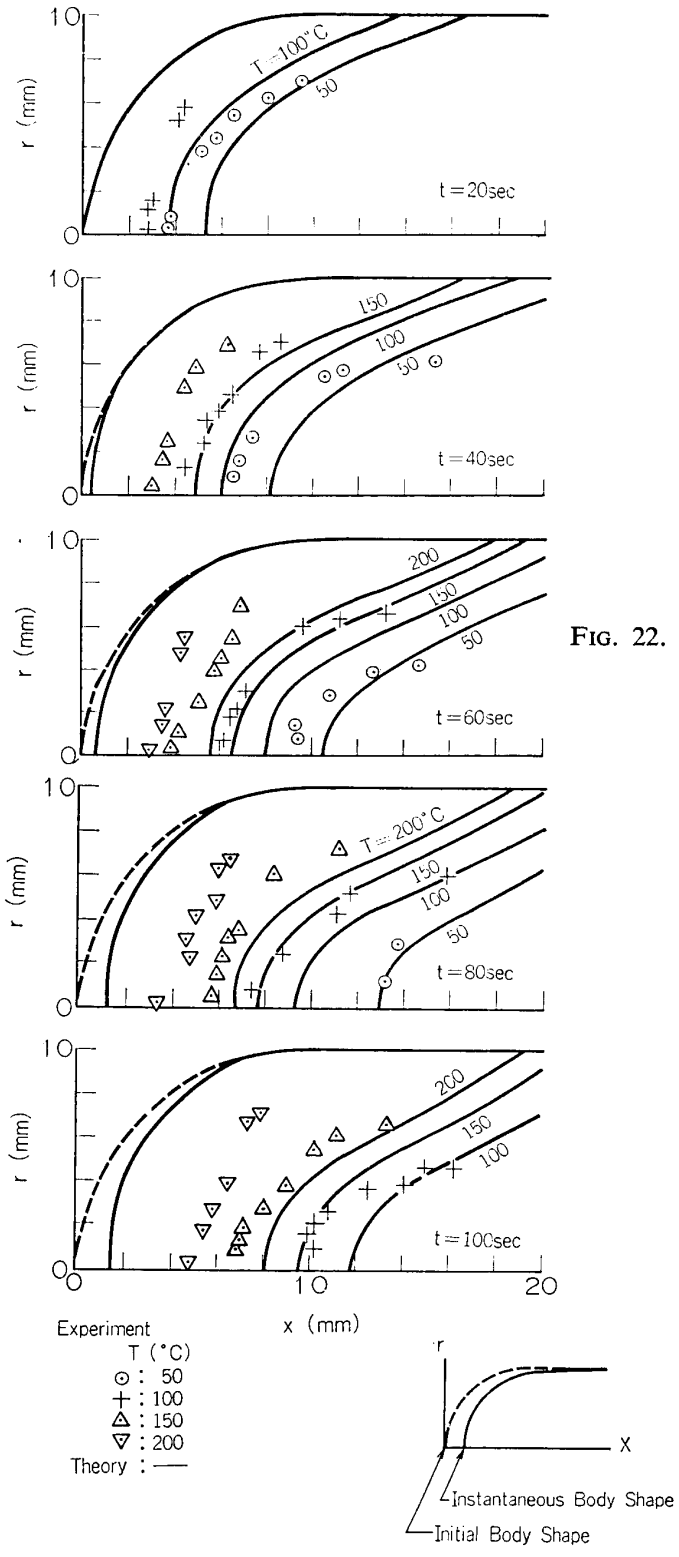

FIG. 22. Instantaneous Internal Temperature Distribution without Gel Layer. $M_\infty=5.74$, $p_{st}=1$ atm, $T_{st}=1020°C$.

the corresponding instantaneous isothermal lines and the results are shown in Fig. 22 together with the experimental data for comparison.

It is remarkable in this figure that the analysis based on the single layer model cannot give a correct prediction of the real thermal field in the ablating body

quantitatively and even its qualitative agreement with the experiment is unsatisfactory.

Therefore, it may be concluded that any theoretical approach to transient thermal response of the ablator made of high molecular compound must be developed on the basis of the multi-layer model of the thermal field.

7. Conclusion

A numerical approach has been developed to transient thermal response of ablating blunt bodies of revolution made of high molecular compounds. With particular emphasis laid on the effect of the second-order transition, the formulation was made by use of a two-layer thermal model and the numerical computation was carried out for a model made of Teflon.

It was shown that the existence of the gel layer has a substantial effect of reducing the apparent thermal diffusivity of the material, resulting in the considerable decrease of the internal temperature near the ablating surface compared with the single layer thermal model.

The numerical results revealed a remarkable fact that the thickness of the gel layer decreases with increase of the surface temperature. This turned out small thickness of the thermal layer and, consequently, the increase in effectiveness of heat shield of the gel layer.

The instantaneous internal temperature distribution obtained by use of the two-layer thermal model was shown to be in satisfactory agreement with experimental data, while the results calculated by use of the single-layer thermal model did not give the correct prediction of the real feature of the transient thermal field in the ablating material.

Finally, it was suggested that any thermal analysis of the transient response of ablating bodies made of Teflon should be developed on the basis of the two-layer thermal model.

Acknowledgement

The author would like to express his gratitude to Prof. K. Karashima for his cordial advices and instructive comments upon this work. He also wishes to thank Mr. K. Sato for his valuable advices on the experiment.

Appendix

It must be remarked that the boundary layer flow on an ablating surface is essentially unsteady because of the change in wall conditions with time. However, if the characteristic flow time, which may be defined as the time required for the boundary layer flow to adapt itself to the new perimeteric conditions, is very small compared with the time for change in the perimeteric conditions, the boundary layer flow will be considered as the quasi-steady approximately.

Since any characteristic time is related primarily to the characteristic transfer velocity of the corresponding phenomenon, the subsequent discussion is made for the order estimation of the velocities appropriate either to the boundary layer flow or to the solid material. For convenience' sake, the order estimation is to be carried out under the conditions listed below;

$$T_{st}=1000^{\circ}\mathrm{C}, \quad T_w=600^{\circ}\mathrm{C}, \quad p_{st}=1\ \mathrm{atm}, \quad M_\infty=6,$$
$$R_b=10\ \mathrm{mm}, \quad \mathrm{Re}_D=10^5,$$

where the nomenclature should be referred to the symbol list. It must be noted that these conditions do not differ so much from those used in the present approach.

The characteristic transfer velocities for convection v_{BV}, diffusion v_{BD} and conduction v_{BC} appropriate to the boundary layer flow can be estimated, respectively, as

$$\left.\begin{aligned} v_{BV} &\sim \frac{\nu}{\delta} \sim O(10^3) \quad (\mathrm{cm}\cdot\mathrm{sec}^{-1}), \\ v_{BD} &\sim \frac{D_g}{\delta} \sim O(10^3) \quad (\mathrm{cm}\cdot\mathrm{sec}^{-1}), \\ v_{BC} &\sim \frac{\alpha_g}{\delta} \sim O(10^3) \quad (\mathrm{cm}\cdot\mathrm{sec}^{-1}), \end{aligned}\right\} \tag{A.1}$$

where ν, D_g and α_g denote kinematic viscosity, binary diffusion coefficient and thermal diffusivity of the flow, respectively, and δ is the boundary layer thickness.

On the other hand, the order of magnitude of the characteristic transfer velocity v_{sc} for the temperature diffusion inside the solid material and the recession rate of the ablating surface which is the characteristic velocity for the change in body shape may be given, respectively, as

$$\left.\begin{aligned} v_{sc} &\sim \frac{\alpha_s}{\delta_T} \sim O(10^{-2}) \quad (\mathrm{cm}\cdot\mathrm{sec}^{-1}), \\ \frac{ds}{dt} &\sim O(10^{-3}) \quad (\mathrm{cm}\cdot\mathrm{sec}^{-1}), \end{aligned}\right\} \tag{A.2}$$

where α_s and δ_T denote thermal diffusivity and thickness of thermal layer inside the body.

It is clear from these results that the characteristic transfer velocities appropriate to the boundary layer flow are considerably large compared with those of the solid material. This, in turn, leads to the statement that the boundary layer flow on the ablating surface can adapt itself very abruptly to the change in surface conditions, thus confirming the validity of the quasi-steady assumption pertinent to the boundary layer flow.

Department of Aerodynamics
Institute of Space and Aeronautical Science
University of Tokyo, Tokyo
July 7, 1976

REFERENCES

[1] Hains, F. D.: "Equilibrium Shape of an Ablating Nose in Laminar Hypersonic Flow," AIAA J., vol. 8, no. 7, 1970, pp. 1354–1355.

[2] Adams, M. L.: "Recent Advances in Ablation," ARS J., vol. 29, 1959, pp. 625–632.

[3] Marvin, J. G. and Pope, R. B.: "Laminar Convective Heating and Ablation in the Mars Atmosphere," AIAA J., vol. 5, no. 2, 1965, pp. 240–248.

[4] Simpkins, P. G.: "On the Stable Shape of Subliming Bodies in a High-Enthalpy Gas Stream," J. Fluid Mechanics, vol. 15, no. 1. Jan. 1963, pp. 110–132.

[5] Newman, R. L.: "A Kinetic Treatment of Ablation," J. Spacecraft, vol. 2, no. 3, 1965, pp. 449–452.

[6] Steg, L.: "Materials for Re-Entry Heat Protection of Satellites," ARS J., vol. 30, no. 9, Sept. 1960, pp. 815–822.

[7] Benjamin, A. S.: "The Effect of Ablative Geometry Change on the Heating and Recession Characteristics of Sphere-Cone," AIAA Paper No. 66–992, 1960.

[8] Karashima, K., Kubota, H., and Sato, K.: "An Aerodynamic Study of Ablation Near the Region of Stagnation Point of Axially Symmetric Bodies at Hypersonic Speeds," Inst. Space and Aero. Sci., University of Tokyo, ISAS Report 425, 1968.

[9] Diaconis, N. S., Fanucci, J. B., and Sutton, G. W.: "The Heat Protection Potential of Several Ablation Materials for Satellite and Ballistic Re-Entry Into the Earth's Atmosphere," G.E.Co., M.S.V.D., TIS No. R59SD423, Sept. 1959.

[10] Scala, S.: "A Study of Hypersonic Ablation," G.E.Co., M.S.V.D., TIS No. R59SD438, Sept. 1959.

[11] Friedman, H. A. and McFarland, B. L.: "Two-Dimensional Transient Ablation and Heat Conduction Analysis for Multimaterial Thrust Chamber Wall," J. Spacecraft Rockets, vol. 5, no. 7, July 1968, pp. 753–761.

[12] Popper, L. A., Toong, T. Y., and Sutton, G. W.: "Three-Dimensional Ablation Considering Shape Changes and Internal Heat Conduction," AIAA Paper No. 70–199, 1970.

[13] Tompkins, S. S., Moss, J. N., Pittman, C. M., and Howser, L. M.: "Numerical Analysis of the Transient Response of Ablating Axisymmetric Bodies Including the Effects of Shape Change," NASA TN D-6220, 1971.

[14] Nomura, S.: "Measurements of Transient Ablation of Teflon," (in Japanese) National Aerospace Laboratory, NAL TR-179, 1969.

[15] Landau, H. G.: "Heat Conduction in a Melting Solid," Quart. Appl. Math., vol. 8, no. 1, 1950, pp. 81–94.

[16] Lees, L.: "Laminar Heat Transfer Over Blunt-Nosed Bodies at Hypersonic Flight Speeds," Jet Propulsion, vol. 26, no. 4, 1959, pp. 259–269, 274.

[17] Swann, R. T., Pittman, C. M., and Smith, J. C.: "One-Dimensional Numerical Analysis of the Transient Response of Thermal Protection Systems," NASA TN D-2976, 1965.

[18] Gross, J. F., Hartnett, J. P., Masson, D. J., and Gazley, C., Jr.: "A Review of Binary Laminar Boundary Layer Characteristics," Int. J. Heat Mass Transfer, vol. 3, 1961, pp. 198–221.

[19] Swann, R. T. and South, J.: "A Theoretical Analysis of Effects of Ablation on Heat Transfer to an Arbitrary Axisymmetric Body," NASA TN D-741, 1961.

[20] Rubesin, M. W. and Inouye, M.: "A Theoretical Study of the Effect of Upstream Transpiration Cooling on the Heat-Transfer and Skin-Friction Characteristics of a Compressible, Laminar Boundary Layer," NACA TN 3969, 1957.

[21] Bartlett, E. P., Nicolet, W. E., and Howe, J. T.: "Heat-Shield Ablation at Superorbital Re-Entry Velocities," AIAA Paper No. 70–202, 1970.

[22] Kemp, N. H.: "Surface Recession Rate of an Ablating Polymer," AIAA J., vol. 6, no. 9, Sept. 1968, pp. 1790–1791.

[23] Rashis, B. and Hopko, R. N.: "An Analytical Investigation of Ablation," NASA TMX-300, 1960.

[24] Wentink, T., Jr.: "High Temperature Behavior of Teflon," Avco. Research Lab. Rept. 55, 1959.

[25] Peaceman, D. W. and Rachford, H. H.: "The Numerical Solution of Parabolic and Elliptic Differential Equations," J. Soc. Indust. Appl. Math., vol. 3, no. 1, March 1955, pp. 28–41.

[26] Siegle, J. C., Muus, L. T., Lin, T., and Larson, H. A.: "The Molecular Structure of Perfluorocarbon Polymers. II. Pyrolysis of Polytetrafluoroethylene," J. Polymer Science, pt. A, vol. 2, no. 1, Jan. 1964, pp. 391–404.

[27] Friedman, H. L.: "The Mechanism of Polytetrafluoroethylene Pyrolysis," G.E.Co., M.S.V.D., TIS No. R59SD385, June 1959.

[28] 辛島桂一，佐藤　清，新井紀夫: "テフロンの非定常アブレーションの実験"，第19回宇宙科学技術連合講演会，大阪，1975.